

Simulations in Support of the Salt Defense Disposal Initiative (SDDI): Water and Salt Transport Driven by Heat Generating Nuclear Waste in Bedded Salt – 14512

Philip Stauffer *, Bruce Robinson *, Roger Nelson **, Dylan Harp *, Amy Jordan *, Hakim Boukhalfa *, Yassin Laybed *, James Ten Cate *

* Los Alamos National Laboratory

** US DOE

Unclassified Los Alamos Document: LA-UR-13-27584

ABSTRACT

Results are presented from simulations performed in support of the Salt Defense Disposal Initiative (SDDI), a field test designed to confirm the behavior of bedded salt as a geologic disposal medium for defense high-level waste (HLW). The SDDI emplacement concept is to place remotely handled waste canisters on the floor of disposal room drifts and cover them with run-of-mine (RoM) salt. Multiphase numerical modeling is used to gain insight into the dominant heat and mass transport processes that are driven by heat generating HLW buried in bedded salt. Findings show that during the proposed 2 year SDDI test, formation of a heat pipe and subsequent salt redistribution are controlled by a combination of high heat load (>500 W per canister, leading to boiling conditions around the heat source), accessible water (>0.5 wt%), and high capillary suction in the RoM backfill. Highly active heat pipes lead to a rind of dry, low porosity salt (<5%) deposited around the canisters with a dissolution band located near the top of the RoM backfill where porosity in the simulations increases above initial values. The dried out low porosity region is coincident with temperatures above boiling (>110C), while the high porosity region is found across the boiling line where water condenses out of the vapor phase, dissolving RoM backfill. Simulations of low heat loads (<500 W, representing over 90% of the EM managed HLW) show almost no salt mass redistribution and very little movement of water during simulations of the proposed SDDI test.

INTRODUCTION

DOE Office of Environmental Management (DOE-EM) is currently planning the Salt Defense Disposal Initiative (SDDI) experiment [1], a field test designed to confirm the behavior of bedded salt as a geologic disposal medium for defense high level waste (HLW) and spent nuclear fuel (SNF). The SDDI test will extend knowledge accumulated during the licensing and operation of the Waste Isolation Pilot Plant (WIPP) by testing a new disposal concept for emplacement of heat-generating radioactive waste. In previous studies [2,3], a waste-disposal concept called the alcove disposal method was introduced. However, because the HLW and defense SNF waste canisters being targeted in the SDDI are not as hot as those associated with commercial HLW, an alternative concept called the in-drift disposal method has been developed in which the waste canisters are placed along the length of a drift, one at a time, and covered with salt backfill for shielding.

Past field heater tests, performed at WIPP, other U.S. salt sites, and worldwide, have provided significant benefit to our knowledge of salt behavior. Previous studies [4,5] have synthesized the information from these tests to evaluate the completeness of our understanding, so that an accurate assessment of the need for future field testing could be evaluated. Callahan et al. [4] concluded that despite the fact that significant

thermal testing has been conducted in both bedded and domal salts both in the U.S. and Germany, there is a gap in our experience base regarding the way in which bedded salt such as that at the WIPP site would behave for the in-drift disposal concept, either for intermediate or high heat loads.

Past work on modeling nuclear waste disposal in salt has been limited by the capability of models to handle highly coupled Thermal-Hydrological-Mechanical-Chemical (THMC) processes. Furthermore, these processes are not completely quantified or understood for the temperature regime in question for HLW. Studies that have laid the foundation for ongoing research to fill science gaps of relevance to HLW disposal in bedded salt are outlined in Hansen and Leigh [6], [2], and Kuhlman and Malama [7]. Previous modeling work completed as part of the SDDI project, including benchmarking simulations against experimental data, is presented in Stauffer et al. [8,9] and Harp et al. [10].

Modeling fluid migration around heated waste is critical for understanding transient thermal, hydrological, and rheological states of the repository system. Water found in bedded salt geologic formations can occur as inter-crystalline inclusions (which are brine pockets present in the boundaries between salt crystals and fractures), intra-crystalline (which are brine inclusions of a few microns to larger than several millimeters present within the crystal structure), and water associated with accessory minerals present in salt such as clay or structural water within secondary mineral structures in the salt such as carnallite, kieserite, gypsum, polyhalite and clay. The total water content in bedded salt varies between 0.5 and few wt. % due primarily to clay content. As the salt is heated above 65°C, water is liberated from accessory minerals and is free to migrate through porosity and fractures [11]. Free water contained in bedded salt is projected to flow towards excavated drifts along pressure gradients. This transport will be driven by both far-field lithostatic pressure and capillary pressure due to drying at the drift walls. Within the drifts, water in the backfill covering waste canisters may reach boiling and be transported as vapor. Further, water in equilibrium with bedded salt at 30°C contains over 300 g/L of dissolved salt, which may be left behind as a precipitate when the water boils off, contributing to porosity change in the boiling region [9]. Understanding the highly coupled physical processes involving water and salt transport around hypothetical heat generating waste packages in bedded salt is a necessary step in possible future proposals for disposal of HLW in salt. Liquid brine flow towards the heat source, establishment of a potential heat pipe in the mine-run salt backfill, boiling, and vapor condensation all lead to changes in porosity, permeability, saturation, thermal conductivity, and rheology of the salt surrounding waste canisters. In short, the interplay of these various processes, especially water liberation and migration, is currently unknown and requires further study.

We begin by presenting a summary of the coupled processes that are used in the simulations of the SDDI, including new algorithms implemented specifically for this project within the LANL developed porous flow simulator, FEHM (e.g., water vapor pressure as a function of both salt concentration and temperature). Next, the numerical model is used to make predictions of temperatures, porosity changes, and saturations that may occur for waste emplaced using the in-drift concept. Simulations include the most complex coupled THC analyses to date, including porosity change as salt dissolves and/or precipitates, boiling of salt water and dry-out, and production of water from clay minerals.

METHODS

The Finite Element Heat and Mass Transfer Code, FEHM, has been developed by LANL for more than 30 years [12]. The code started as a tool to simulate geothermal reservoirs as part of LANL's groundbreaking

Hot Dry Rock geothermal energy program (Kelkar et al., 2011), but has grown over the years to include unsaturated flow, reactive chemistry, stress, and carbon dioxide (<https://fehmlanl.gov>). FEHM has been used in research studies in more than 100 peer reviewed publications [13]. FEHM uses a finite volume method for solving multiphase flow and transport, while using a finite element formulation for the fully coupled stress solutions. Capabilities pertinent to the salt simulations presented in this report include the ability to run fully coupled heat and mass transfer on both 2-D radial and 3-D numerical meshes. We also make use of the reactive chemistry module of FEHM, allowing us to modify porosity caused by dissolution and precipitation and explore mineral dehydration reactions including associated release of water during heating. In the rest of this chapter, we describe additions to FEHM allowing simulation of fully coupled THC processes in salt. These additions to the code make FEHM uniquely capable for addressing the questions concerning water migration during the SDDI heater test.

In the FEHM simulations presented, we ignore the large-scale deformation processes due to salt creep that will dramatically impact the long-term sealing of the repository. Therefore, our results are relevant to the evolution of the thermal regime and water transport processes during the initial heat-up and final cool-down of the proposed SDDI two year test. In the subsections that follow, the constitutive relationships and other model issues specific to the modeling the thermal, hydrologic, and chemical behavior of a salt repository are described.

Salt related algorithms in FEHM

Thermal Conductivity of Salt as a Function of Porosity and Temperature

Thermal conductivity of salt can change dramatically with changes in porosity and temperature. Munson et al. [14] investigated the temperature dependence of the thermal conductivity (k_t [W/m/K]) of intact salt at the Waste Isolation Pilot Plant (WIPP), identifying the following relationship:

$$k_{t-WIPP}(T) = k_{t-300} \left(\frac{300}{T} \right)^{1.14} \quad (1)$$

where k_{t-300} is the thermal conductivity at 300 K (5.4 W/m/K) and T is temperature in Kelvin. Bechthold et al. [15] investigated the dependence of thermal conductivity on porosity of RoM salt at the Asse salt mine in Germany. They developed the following relationship fitting the thermal conductivity of RoM salt to porosity (ϕ) using a fourth-order polynomial:

$$K_{T-ASSE}(\phi) = -270\phi^4 + 370\phi^3 - 136\phi^2 + 1.5\phi + 5 \quad (2)$$

In order to combine the findings of Munson et al. and Bechthold et al. [14,15], K_{T-ASSE} has been scaled to match K_{T-300} at $\phi=0$ as

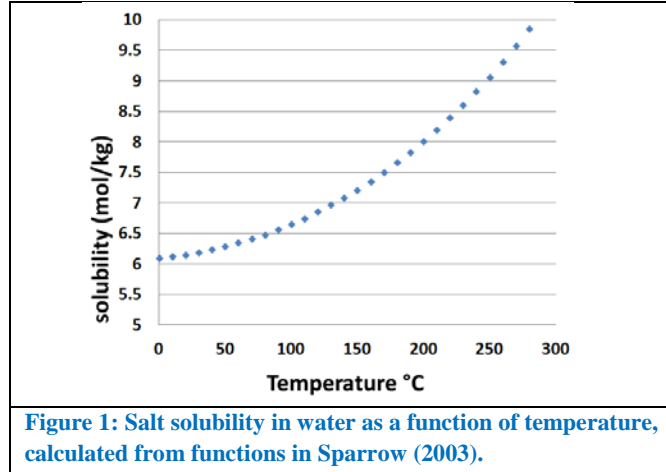
$$K_{T-300}(\phi) = \left(\frac{K_{T-300}}{K_{T-ASSE}(\phi=0)} \right) * K_{T-ASSE}(\phi) \quad (3)$$

where $K_{T-300}/K_{T-ASSE}(\phi=0)$ is 5.4/5.0, or 1.08. Equations 1 and 2 have been derived using data from domal and bedded salt formations, respectively. The relationship of thermal conductivity to temperature and porosity may not be the same in these formations. Following Clayton and Gable [16], the assumption has been made here that RoM salt has the same temperature dependence as intact salt, giving

$$K_{T-crushed}(T, \phi) = K_{T-300}(\phi) \left(\frac{300}{T}\right)^{1.14}. \quad (4)$$

Salt solubility as a function of temperature

The solubility of salt is calculated in FEHM by a simple function shown in Figure 1, derived from Sparrow [17].



Precipitation/Dissolution of Salt

In this model, precipitation and dissolution reactions of NaCl result in changes in the porosity of the salt medium. Precipitation and dissolution are explicitly coupled to the heat and mass transfer solution through feedbacks on porosity, permeability, thermal conductivity, and vapor pressure. Changes in porosity ($\Delta\phi$) are calculated at each node, following each chemistry iteration as:

$$\Delta\phi_i = \Delta c \rho_s m_s \frac{1}{\rho_{NaCl}} (1 - \phi_i), \quad (5)$$

where $\Delta c = c_i - c_{i-1}$ is the change in the moles of solid NaCl per weight of the solid [kg], ρ_s is density of the solid [kg/m³], m_s is the molar mass of NaCl [kg/mol], ρ_{NaCl} is the density of NaCl [kg/m³], and i is a solute transport solution iteration index. We further assume $\rho_s = \rho_{NaCl}$.

Water vapor diffusion coefficient as a function of pressure, temperature, and porosity

Water vapor diffusion is modified to account for thermal and pressure effects through the following equation (modified from Zvyoloski et al., [18]).

$$D_{va} = \tau D_{va}^0 (P_o/P) ((T+T_o)/T_o)^\theta \quad (7)$$

where τ = tortuosity, $D_{va}^0 = 2.23 \times 10^{-5}$, $T_o = 273.15$ K, $\theta = 1.81$, T = temperature in C, P = pressure in MPa, and $P_o = 0.1$ MPa. The effective free air water vapor diffusion coefficient is then modified using the Millington-Quirk relationship where τ is calculated as:

$$\tau = (S_v^* \phi)^{2.333} / \phi^2 \quad (8)$$

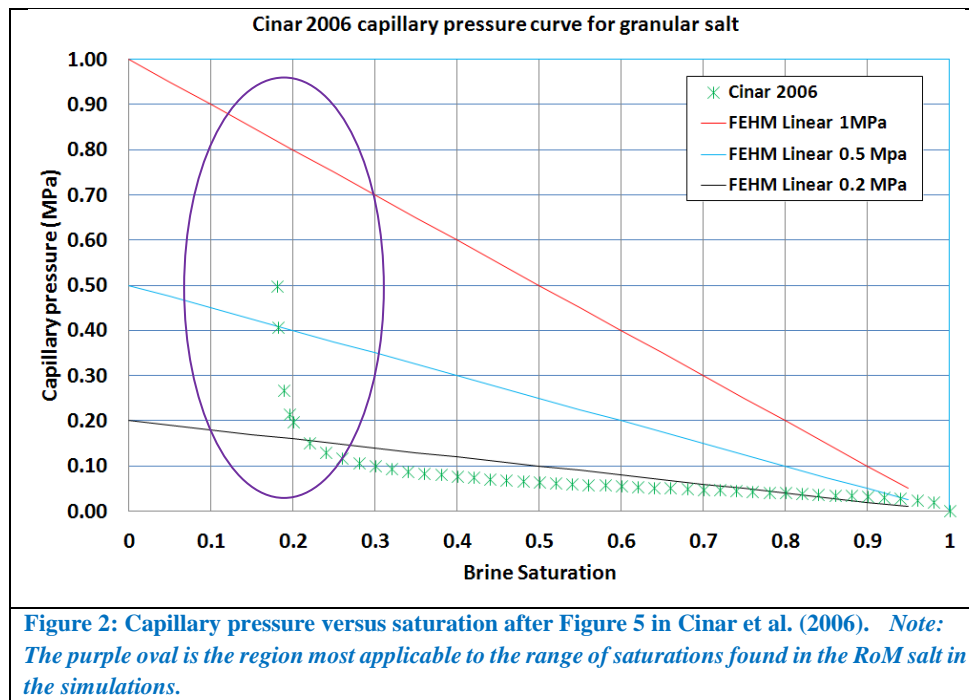
where S_v = air saturation. The resulting vapor diffusion coefficient is implemented in the mass transport equation for diffusion of water vapor through air driven by a concentration gradient in the bulk vapor phase (air + water vapor) as:

$$mf_{wv} = -D_{va} f S_v m_{wv} \nabla C_{wv} \quad (9)$$

where mf_{wv} = mass flux of water vapor, m_{wv} = molecular weight of water vapor (kg/mol) and C_{wv} = moles of water vapor per cubic meter of air. In Equation (9), mf_{wv} reduces to units of kg/(m² s).

Capillary pressure relationships

Limited data on the capillary pressure of granular salt versus saturation are available in the literature. We rely on Cinar et al. [19] to guide our choice of which capillary pressure values to use in our simulations. As seen in Figure 2, the measured data for granular salt suggest capillary suction of greater than 0.5 MPa at dry conditions. Although the cases are unequal in their ability to match the data at the wet end of the curves ($S > 0.2$), for the low end of saturation (<0.2 MPa), the range most relevant to these simulations, these three functions lie across the measured data.



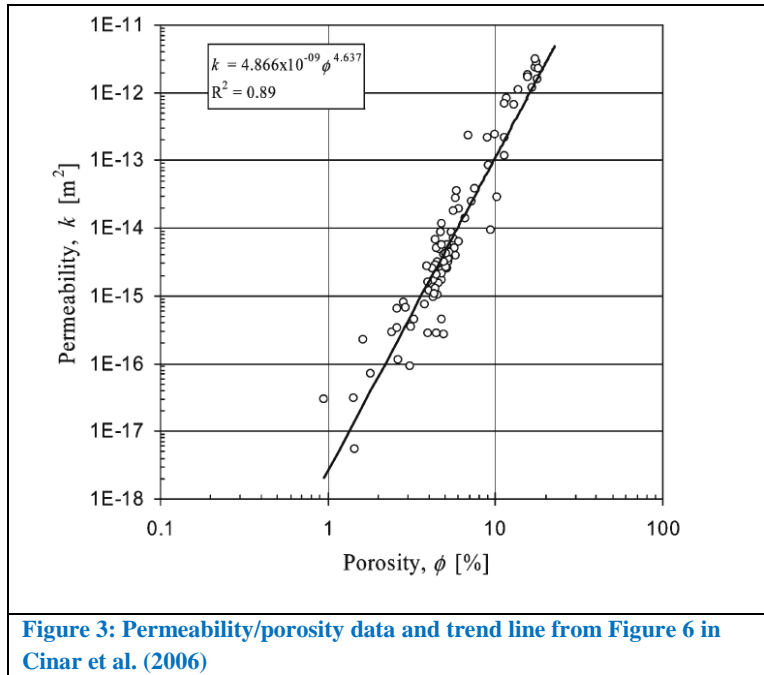
Permeability-Porosity Relationship for RoM Salt

Cinar et al. [19] identified a permeability-porosity relationship based on measurements of compacted pure sodium chloride. A generalized form of this relationship was implemented into FEHM as

$$k = \begin{cases} c_1 \phi_l^{c_2} & \text{if } \phi < \phi_l \\ c_1 \phi^{c_2} & \text{if } \phi_l \leq \phi \leq \phi_u \\ c_1 \phi_u^{c_2} & \text{if } \phi > \phi_u \end{cases} \quad (10)$$

where k is permeability (m^2), ϕ_l and ϕ_u are the upper and lower porosity limits for the relationship, respectively, and c_1 and c_2 are fitting parameters.

The user specifies the upper and lower porosity limits and fitting parameters. For the simulations presented here, the values of c_1 and c_2 from Cinar et al. [19] of 4.866×10^{-9} and 4.637, respectively, are used (refer to Figure 3). The upper and lower porosity limits were set to 0.2 and 1×10^{-6} , respectively. This lower limit is an extrapolation beyond the data presented in Cinar et al. [19]. This model does not include the compaction of RoM salt, but instead simulates only the dissolution and precipitation of NaCl, for which it is assumed that the relationship depicted in Figure 3 is valid.



Vapor Pressure of Water as a function of Aqueous Sodium Chloride Concentration and Temperature

The vapor pressure of water depends on the dissolved salt concentration, with higher concentrations resulting in lowered vapor pressures. Sparrow [17] developed polynomial equations relating vapor pressure (P_v) to the salt mass fraction and temperature.

Figure 4, from Sparrow (2003), presents vapor pressure as a function of salt mass fraction and temperature.

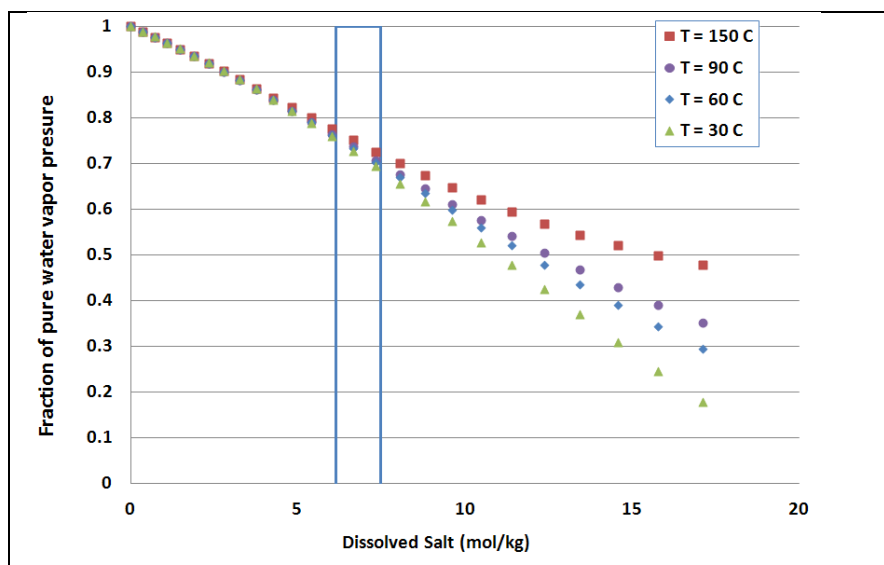


Figure 4 Vapor pressure lowering fraction as a function of salt concentration and temperature. The blue box represents the range of values expected in the SDDI test.

Clay Dehydration

Hydrous mineral dehydration reactions have the possibility of impacting the evolution and transport of water in a salt repository, so models must be developed to capture these effects, including the temperature dependent introduction of water into the pore space, where it is available to transport and react with the solid salt. FEHM has been modified to provide a water source from dehydration of clay impurities in salt, based on preliminary experimental data from WIPP samples with varying clay content [9,11].

As implemented in FEHM, the clay dehydration model can be applied to selected nodes or zones within the model, and differing clay fractions can be specified. Based on the experimental information available, at 64°C, 14.8% of the mass of clay in the node is added as a source term in a one-time release of water. At 110°C, 2.5% of the clay mass is released as water, and at 264°C, an additional 6.7% is released.

The current clay dehydration model does not distinguish between water released by clay dehydration and that produced by other bound water sources such as fluid inclusion migration to a grain boundary. In the future, it is possible that all crushed salt nodes will utilize the “clay dehydration” model to release water from fluid inclusions. In the low-porosity intact salt, water production might raise fluid pressures and influence hydraulic fracturing. On the other hand, water production in intact salt will be most significant at the clay seams, where shrinkage could occur during dehydration, producing additional porosity for the produced water. These issues will be the subject of future work.

Drift scale heater test simulation design

The 3-D numerical mesh built for exploring options for a field-scale thermal test contains 117,670 nodes with high resolution in the RoM salt to allow accurate delineation of boiling fronts that move through time and space. The three-dimensional mesh is a ¼ space representation of the true domain, with reflection boundaries on both faces shown in Figure 5. The mesh extends from -18.3 to +18.3 m (120 ft) in the z direction, from 0.0 to 18.3 m (60 ft) in the y direction, and from 0.0 to 12.2 m (40 ft) in the x direction. The drift is 3.0 m (10 ft) high and the pile of RoM salt is 1.8 m (6 ft) high. The damaged rock zone (DRZ) is 1.5

m (5 ft) thick surrounding the drift. Material properties and/or initial conditions used in these simulations are shown in Table 4.

The simulations are started from an initial state where the fixed far-field pressure of 15 MPa is allowed to begin equilibrating with the drift pressure set to atmospheric pressure (0.1 MPa). The temperature in the background runs is fixed at 30°C. The saturation in the RoM salt is varied from 0.01 to 0.1, equivalent to a water fraction by mass of 0.25% to 2.5% (mass water/mass total). The background runs allow saturation in the DRZ to drop slightly during the initialization period of 60 days, as water is pulled from the DRZ into the RoM salt. These initial states are used to start simulations with different combinations of heat loads, capillary pressures, initial saturation in the RoM salt, and clay fractions in the RoM salt.

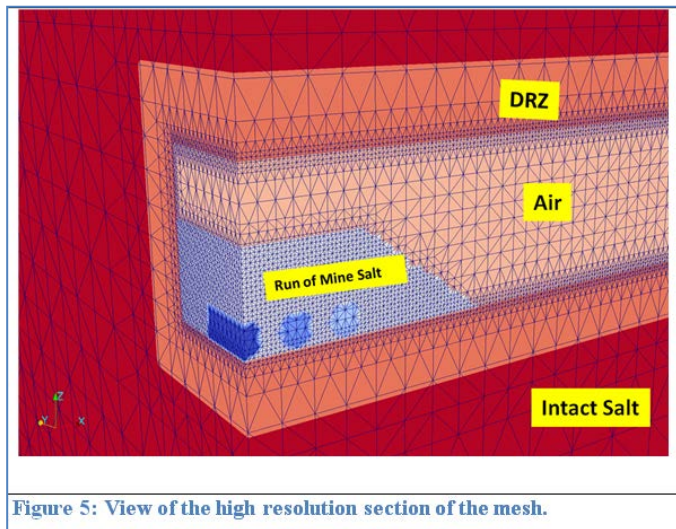


Figure 5: View of the high resolution section of the mesh.

Table 1: Material properties and/or initial conditions for the THC model runs

	Canister	RoM Salt	Air	DRZ	Intact salt
Density	2230.	2165.	2165.	2165.	2165.
Thermal cond.	1.1	variable	14.0	variable	variable
Heat capacity	710.	931.	0.46	931.	931.
porosity	0.00001	variable 0.35 initial	0.999	0.01	0.001
Saturation	1e-5	0.01 to 0.1	1e-6	1 initial	1
Permeability (m ²)	10 ⁻²¹	variable	10 ⁻¹¹	10 ⁻¹⁹	10 ⁻²¹
Max capillary pressure (MPa)	0.1	0.1 to 1.0	0.001	0.1 to 1.0	0.1 to 1.0
Solubility reaction	NO	YES	YES	NO	NO
Clay mass fraction	0	0 – 10%	0	0	0

Solid salt is modeled as having 17.11 moles of salt per kilogram. Initial concentration of salt in the water comes from the solubility relationship and yields 6.16 mol of salt per kg of water at 30°C.

All simulations of drift heating are run to two years, the assumed length of the heater test. The boiling point in salt-saturated solutions is elevated with respect to pure water, and in our simulations occurs at around 109°C. The total volume of the RoM salt pile is 14.4 m³, and the initial mass of water in this zone at 10% saturation is 500 kg.

DISCUSSION

Thermal-Hydrologic-Chemical (THC) Simulations of a Field Scale Heater Test

Porosity change as a function of heat load

Results for the fully coupled THC simulations show that a range of behavior can occur in the RoM salt based on availability of both water and heat. One of the primary indicators of changes in behavior is porosity change from the initial 35% (35% is indicated as yellow in the porosity figures below). Figures 6(A,B,C) illustrate the types of porosity change seen in different simulations; in these figures the only parameter varied was the heat load in the canisters. For heat loads of 250W, 500W and 750W, the porosity changes are significantly enhanced for higher heat loads. In all cases there is little water flowing into the RoM salt from the DRZ, the initial saturation of the RoM pile is 10%, and the maximum capillary suction in the RoM salt is 1.0 MPa. As a metric for porosity change, we use the following: $PC_{tot} = \text{sum over all RoM nodes (abs(initial porosity} - \text{final porosity))}$. This metric produces a volume of porosity change and sums both gains and losses. For case A, this value is 0.16 m^3 , for case B it is 0.46 m^3 , while for case C, $PC_{tot} = 1.18 \text{ m}^3$.

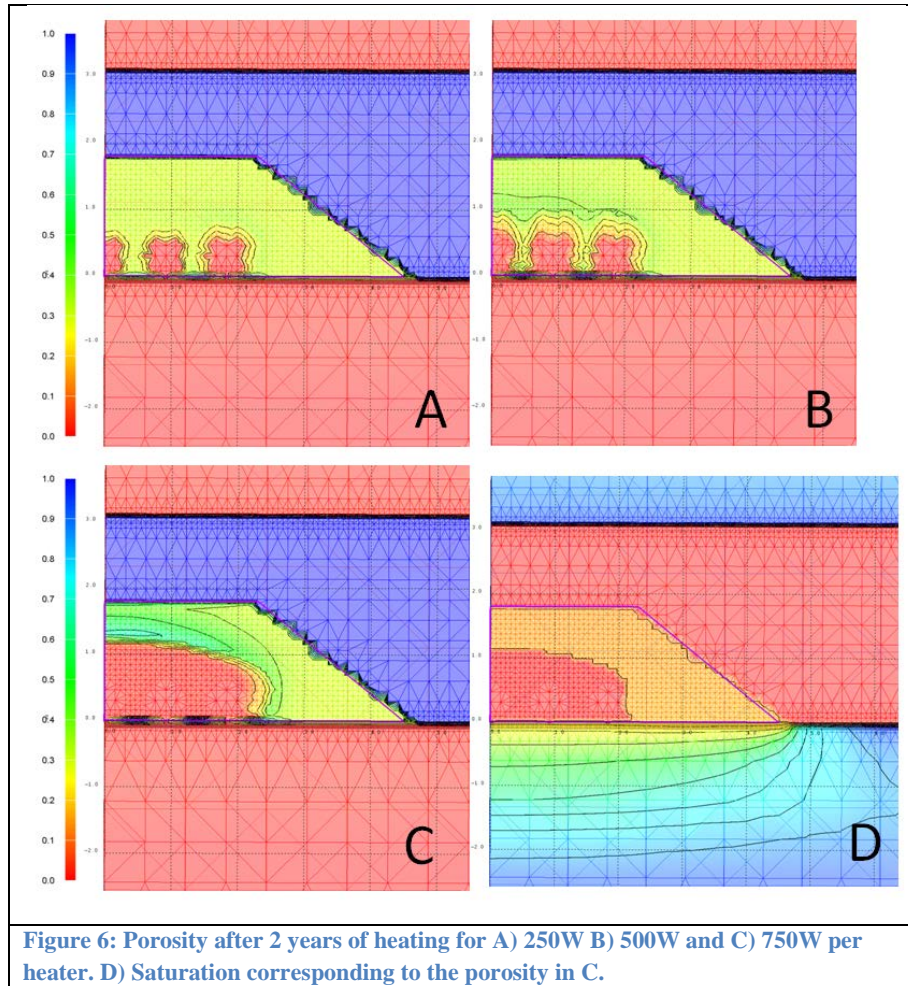
Temperature versus time at locations on the line of maximum temperature ($x=0, y=0$) show that the middle of the RoM salt reaches only 60°C in the 250W case, while reaching near 110°C in the 750W case. Although the 500W case did not reach boiling at the edge of the canister, there was still enough vapor transport and recirculation of condensate to lead to intermediate porosity change ($PC_{tot} = 0.46$).

The large changes in porosity seen in the 750W case are caused by the creation of a heat pipe that pushes purified water vapor away from the heat and pulls saturated brine back towards the heat by capillary suction from wetter regions to the very dry region that develops around the heaters. The dry-out region can be seen in Figure 6D.

Although tests have not been performed in this configuration, there is experimental evidence for mass redistribution and porosity change in heated salt from 1980s heater tests in Room B [20]. Post analysis of these tests discovered that the porosity of the annular region surrounding canisters in boreholes was greatly reduced [20]. The likely cause of the porosity redistribution is heat pipe formation with liquid re-supplied by fluids seeping from the intact salt around the borehole.

Porosity change as a function of initial saturation

Another set of simulations demonstrates the impact of available water on porosity redistribution (Figure 7 A,B, and C). For these three simulations, the heat load is constant at 750W per canister and the maximum capillary suction in the RoM salt is 0.5 MPa. In these simulations, the maximum temperature is higher in the dry cases, with the 1% saturation leading to maximum temperature of 192°C at 2 years, while the 10% saturation case reaches only 145°C .



In all of these cases the dry-out region is approximately the same as seen in Figure 6D, with the drier initial condition simulations having slightly larger dry-out envelopes. The PC_{tot} for these cases is A = 0.22 m³, B = 0.19 m³, C = 0.38 m³, D = 1.17 m³. Interestingly, the temperature profiles are consistent for most of the domain, deviating only near the waste canisters, with marked differences between the wet initial condition that created a heat pipe and the other initial states that do not.

Porosity change as a function of capillary suction in the RoM salt

Capillary suction impacts the available water in the RoM salt through interactions with the DRZ beneath the pile. For greater suction, more water can be pulled into the RoM salt, providing more drive for the heat pipe. Similarly, more suction allows the heat pipe to strengthen, as increased suction is more efficient at pulling saturated brine back towards the hot region. For two cases (750W, 10% initial saturation) having the only difference being maximum capillary suction in the RoM salt, 0.5 MPa of suction led to $PC_{tot} = 0.38$ m³ while 0.1 MPa of suction produced $PC_{tot} = 0.29$ m³.

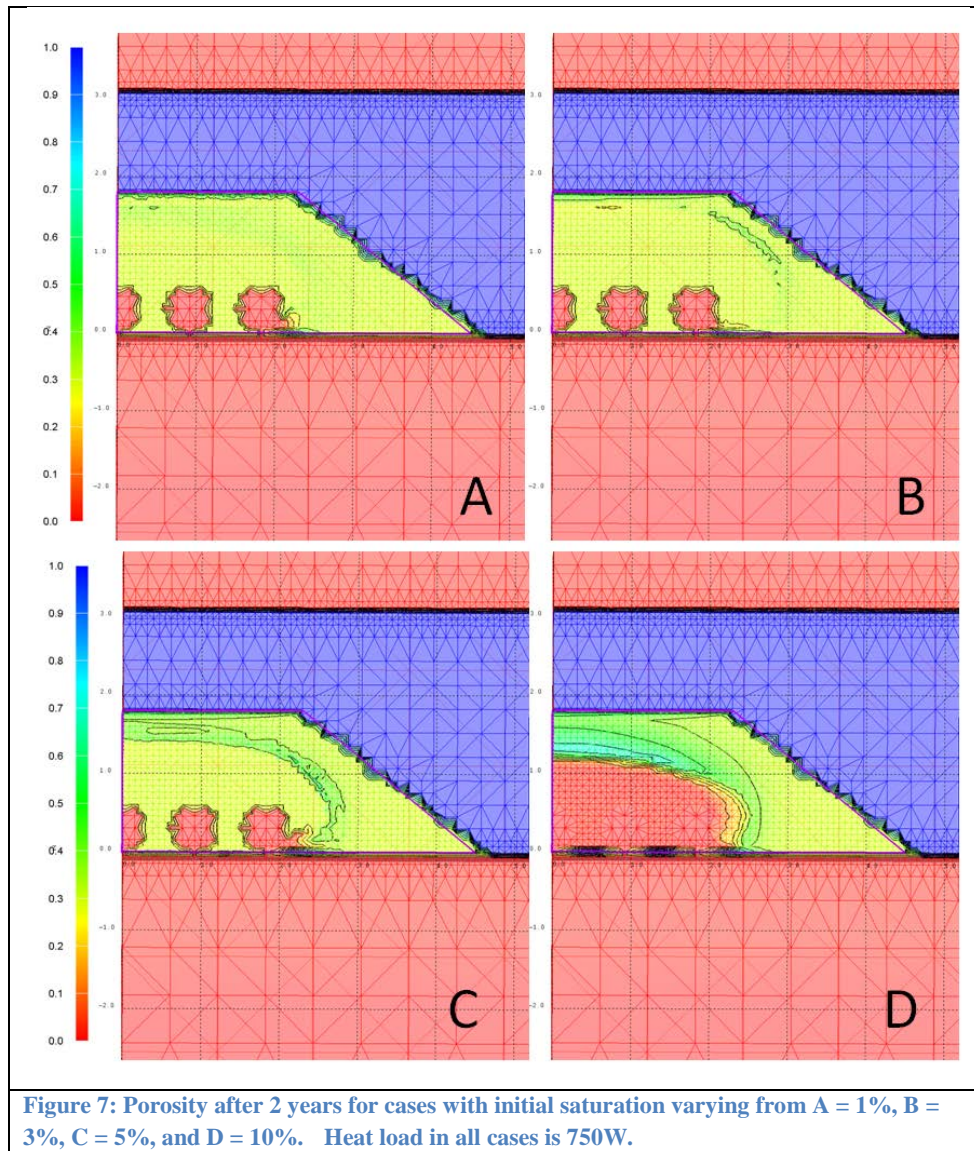
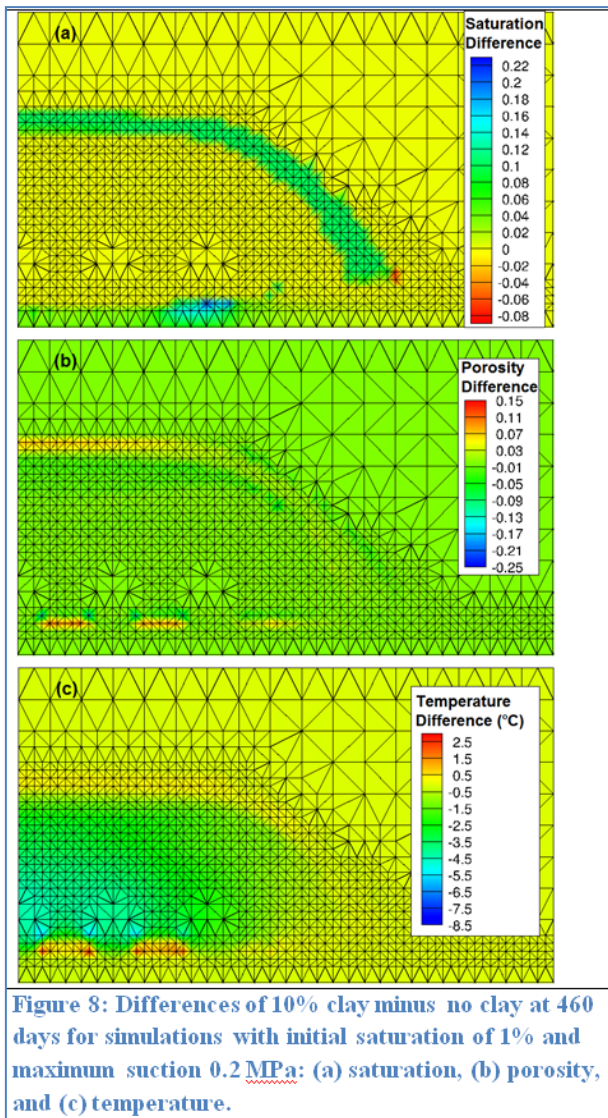


Figure 7: Porosity after 2 years for cases with initial saturation varying from A = 1%, B = 3%, C = 5%, and D = 10%. Heat load in all cases is 750W.

Porosity change as a function of clay fraction

The effect of clay dehydration in the full three-dimensional model was tested and compared to corresponding cases without clay. All simulations in this section use 750W heaters. Clay dehydration was only added in the crushed salt zone, with percentages of clay ranging from 1 to 10% in different simulations.



The saturation, porosity, and temperature differences at 460 days between 10% clay and the corresponding simulation with no clay (both with initial saturation 1% in the crushed salt and 0.2 MPa maximum capillary suction) are shown in Figure 8. The purpose of this comparison is to determine whether the simulated water release from a material with high clay content will make the difference between heat pipe dry-out (as seen in the 1% initial saturation case) and an active heat pipe that contributes to porosity reduction around the heaters. The amount of water produced in the simulation with 10% clay in the crushed salt pile is 119 kg by 460 days. In comparison, the case that starts with 10% initial saturation has ~500 kg more water in the crushed salt than the case with 1% initial saturation. Therefore, the 10% clay case produces an intermediate amount of water and the timing of water release is staggered for the nodes across the crushed salt pile. A ring of higher saturation persists outside the boiling region in the case where clay dehydration releases a source of water, but it is not enough water to sustain a vigorous heat pipe as in the 10% initial saturation case. The porosity difference between the clay and no clay cases, Figure 8(b), shows the small amount of salt buildup (porosity reduction) in the wetter case with clay dehydration, and temperatures are generally cooler for the wetter case, Figure 8(c).

CONCLUSIONS

Coupled Thermal, Hydrological, and Chemical (THC) processes representing a possible test configuration for the Salt Defense Disposal Initiative (SDDI) field test are simulated. Coupled processes include solubility of salt as a function of temperature, clay dehydration, wherein clay minerals release water while undergoing mineralogical changes, boiling of saturated salt water and precipitation of salt, transport of water vapor, condensation of water vapor back to liquid water and subsequent dissolution of salt, thermal conductivity of salt as a function of porosity and temperature, permeability as a function of porosity, and water vapor pressure as a function of salt concentration and temperature. These processes have been added to FEHM, LANL's state-of-the-art porous flow simulator for multiphase thermal problems.

The FEHM model shows that the heating can lead to porosity changes determined mainly by the water content of the Run-of-Mine (RoM) salt used as backfill and the heat load of the waste canisters. Heat loads

on the order of 750W are required to generate heat pipes assuming five canisters with 0.3 m spacing. Secondary impacts on porosity change include the initial clay content of the RoM salt and the capillary suction in this material. Creation of a strong heat pipe in hot, wet cases leads to porosity reduction in a band around the heaters due to boiling and subsequent precipitation of salt from the circulating brine and water vapor. Evidence of heat pipe formation in past heater tests at WIPP in Room B boreholes suggests that the mechanism could be important. Lower temperatures result from higher thermal conductivity where porosity is decreased due to boiling and subsequent precipitation. Threshold initial water content for creation of a heat pipe appears to be between 1.2 and 2.4 wt% water, toward the high end of measured WIPP water contents, but additional work is needed to determine whether a vigorous heat pipe is a realistic expectation for the heater test scenario. Interestingly, drier initial conditions allow more water to be generated by clay dehydration because of higher temperatures further from the simulated waste canisters. Although clay content and capillary suction are second order effects, they could play a deciding role in cases for which the RoM initial saturation is close to threshold heat-pipe conditions.

References

1. DOE Carlsbad Field Office (DOE CBFO), 2012. A Management Proposal for Salt Defense Disposal Investigations (SDDI) for the Disposal of DOE-EM Managed Wastes, U.S. Department of Energy Carlsbad Field Office document, February 2012.
2. Robinson, B. A.; Elkins, N. Z.; Carter, J. T., Development of a U.S. nuclear waste repository research program in salt. *Nuclear Technology* **2012**, *180*, 122-138.
3. Carter, J.T., F.D. Hansen, R. Kehrman, T.A. Hayes. 2011. *A Generic Salt Repository for Disposal of Waste from a Spent Nuclear Fuel Recycle Facility*. Savannah River National Laboratory Report SRNL-RP-2011-00149.
4. Callahan, G., D.C. Guerin, D.G. Levitt, D.L. Newell, B.A. Robinson, L. Van Sambeek. 2012. *Salt Repository Synthesis Data of Non-Delaware Basin and International Programs for the Storage/Disposal of Nuclear Waste*. Los Alamos National Laboratory Report LCO-SDI-002.
5. Kuhlman, K., S. Wagner, D. Kicker, R. Kirkes, C. Herrick, D. Guerin. 2012. *Review and Evaluation of Salt R&D Data for Disposal of Nuclear Waste in Salt*. DOE Office of Nuclear Energy Report FCRD-UFD-2012-000380.
6. Hansen, F.D., and C.D. Leigh. "Salt Disposal of Heat-Generating Nuclear Waste." SAND2011-0161. Albuquerque: Sandia National Laboratories. 2011.
7. Kuhlman, K.L. and Malama, B. (2013). *Brine Flow in Heated Geologic Salt*. SAND2013-1944, Albuquerque, NM: Sandia National Laboratories.
8. Stauffer, P.H., D.R. Harp, B.A. Robinson, (2012) Model Development and Analysis of the Fate and Transport of Water in a Salt-Based Repository, DOE Level 3 Milestone M2FT-12LA08180112, LANL Report LA-UR-12-25050.
9. Stauffer, P.H., D.R. Harp, A.B. Jordan, Z. Lu, S. Kelkar, Q. Kang, J. Ten Cate, H. Boukhalfa, Y. Labyed, P.W. Reimus, F.A. Caporuscio, T.A. Miller, B.A. Robinson, (2013) Coupled model for heat and water transport in a high level waste repository in salt, September 30, 2013 FCRD-UFD-2013-000206 Los Alamos National Laboratory Document LA-UR 13-27584
10. Harp D.R., P.H. Stauffer, P.K. Mishra, D.G. Levitt, and B.A. Robinson (2013). Thermal Modeling of High-Level Nuclear Waste Disposal in a Salt Repository. *Nuclear Technology*, *in press*.

11. Caporuscio, F.A., H. Boukhalfa, M.C. Cheshire, A.B. Jordan, and M. Ding, Brine Migration Experimental Studies for Salt Repositories, September 25, 2013 FCRD-UFD- 2013-000204 Los Alamos National Laboratory Document LA-UR 13-27240.
12. Zyvoloski, G.A.(2007). *FEHM: A control volume finite element code for simulating subsurface multi-phase multi-fluid heat and mass transfer*, Report LA-UR-07-3359, Los Alamos National Laboratory.
13. FEHM. (2012). FEHM reference list, online at http://fehm.lanl.gov/pdfs/FEHM_references_list.pdf, accessed Aug. 31, 2012. .
14. Munson, DE, RL Jones, JR Ball, RM Clancy, DL Hoag and SV Petney. 1990. *Overtest for Simulate Defense High-Level Waste (Room B): In Situ Data Report (May 1984-February 1988) Waste Isolation Pilot Plant (WIPP) Thermal/Structural Interactions Program*, Sandia National Laboratories, SAND89-2671.
15. Bechthold W., Smailos E., Heusermann S., Bollingerfehr W., Sabet B.B., Rothfuchs T., Kamlot P., Grupa J., Olivella S., and Hansen F.D., 2004. Backfilling and sealing of underground repositories for radioactive waste in salt (Bambus II project). Final Report for European Atomic Energy Community EUR 20621, Office for Official Publications of the European Communities, Luxembourg. ISBN 92-894-7767-9.
16. Clayton, D.J. and C.W. Gable, 2009. 3-D Thermal Analyses of High-Level Waste Emplaced in a Generic Salt Repository, Advanced Fuel Cycle Initiative, AFCI-WAST-PMO-MI-DV-2009-000002, SAND2009-0633P. LA-UR-09-0089.
17. Sparrow, B. S., 2003. Empirical equations for the thermodynamic properties of aqueous sodium chloride, *Desalination*, 159, 2, 161-170.
18. Zyvoloski, G.A., B.A. Robinson, Z.V. Dash, and L.L. Trease. 1997. Summary of the models and methods for the FEHM application— A finite-element heat-and mass-transfer code. Rep. LA-13307-MS. Los Alamos National Laboratory, Los Alamos, NM. .
19. Cinar, Y., G. Pusch, and V. Reitenbach, 2006. Petrophysical and Capillary Properties of Compacted Salt, *Transport in Porous Media*, 64, 199-228.
20. Krumhansl, J. L., C. L. Stein, G. D. Jarrell, and K. M. Kimball, 1991. Summary of WIPP Room B heater test brine and backfill material data. SAND90-0626, Sandia National Laboratories, Albuquerque, NM, 1991.